From Permeation to Cluster Arrays: Graphene on Ir(111) Exposed to Carbon Vapor

Herbig, C.; Knispel, T.; Simon, S.; SchröDer, U. A.; MartíNez-Galera, A. J.; Arman, M. A.; Teichert, C.; Knudsen, J.; Krasheninnikov, A. V.; Michely, T.;

Originally published:

April 2017

Nano Letters 17(2017)5, 3105-3112

DOI: https://doi.org/10.1021/acs.nanolett.7b00550

From Permeation to Cluster Arrays: Graphene on Ir(111) Exposed to Carbon Vapor

Journal:	*Nano Letters*
Manuscript ID	nl-2017-00550h.R1
Manuscript Type:	Communication
Date Submitted by the Author:	10-Apr-2017

Complete List of Authors:	Herbig, Charlotte; Universität zu Köln, II. Physikalisches Institut Knispel, Timo; Universität zu Köln, II. Physikalisches Institut Simon, Sabina; Universität Konstanz Schröder, Ulrike; Universität zu Köln, II. Physikalisches Institut Martínez-Galera, Antonio; Universidad Autónoma de Madrid, Departamento de Física de la Materia Condensada Arman, Mohammad; Lund University, Division of Synchrotron Radiation Research Teichert, Christian; Institut für Physik, Montanuniversität Leoben, Knudsen, Jan; Division of Synchrotron Radiation Research and the MAX IV Laboratory, Lund University, Krasheninnikov, Arkady; Helmholtz-Zentrum Dresden-Rossendorf, Ion Beam Centre Michely, Thomas; Universität zu Köln, II. Physikalisches Institut

From Permeation to Cluster Arrays: Graphene on Ir(111) Exposed to Carbon Vapor

Charlotte Herbig,[*,†] Timo Knispel,[†] Sabina Simon,[†,‡] Ulrike A. Schröder,[†] Antonio J. Martínez-Galera,[†] Mohammad A. Arman,[¶] Christian Teichert,[†,§] Jan Knudsen,[‖] Arkady V. Krasheninnikov,[⊥,#] and Thomas Michely[†]

II. Physikalisches Institut, Universität zu Köln, Zülpicher Straße 77, 50937 Köln, Germany, present address: Department of Physics, University of Konstanz, Universittstr. 10, 78464 Konstanz, Germany, Division of Synchrotron Radiation Research, Lund University, Box 118, 22100 Lund, Sweden, permanent address: Institute of Physics, Montanuniversität Leoben, Franz Josef Str. 18, 8700 Leoben, Austria, Max IV Laboratory and Division of Synchrotron Radiation Research, Lund University, Box 118, 22100 Lund, Sweden, and Helmholtz-Zentrum Dresden-Rossendorf, Institute of Ion Beam Physics and Materials Research, 01328 Dresden, Germany

E-mail: herbig@ph2.uni-koeln.de

Abstract

[*]To whom correspondence should be addressed
[†]II. Physikalisches Institut, Universität zu Köln, Zülpicher Straße 77, 50937 Köln, Germany
[‡]present address: Department of Physics, University of Konstanz, Universittstr. 10, 78464 Konstanz, Germany
[¶]Division of Synchrotron Radiation Research, Lund University, Box 118, 22100 Lund, Sweden
[§]permanent address: Institute of Physics, Montanuniversität Leoben, Franz Josef Str. 18, 8700 Leoben, Austria
[‖]Max IV Laboratory and Division of Synchrotron Radiation Research, Lund University, Box 118, 22100 Lund, Sweden
[⊥]Helmholtz-Zentrum Dresden-Rossendorf, Institute of Ion Beam Physics and Materials Research, 01328 Dresden, Germany
[#]Department of Applied Physics, Aalto University School of Science, P.O. Box 11100, 00076 Aalto, Finland

Our scanning tunneling microscopy and X-ray photoelectron spectroscopy experiments along with first-principles calculations uncover the rich phenomenology and enable a coherent understanding of carbon vapor interaction with graphene on Ir(111). At high temperatures, carbon vapor not only permeates to the metal surface, but also densifies the graphene cover. Thereby, in addition to underlayer graphene growth, upon cool down also severe wrinkling of the densified graphene cover is observed. In contrast, at low temperatures the adsorbed carbon largely remains on top and self-organizes into a regular array of fullerene-like, thermally highly stable clusters that are covalently bonded to the underlying graphene sheet. Thus a new type of predominantly sp^2-hybridized nanostructured and ultrathin carbon material emerges, which may be useful to encage or stably bind metal in finely dispersed form.

Keywords

graphene, carbon deposition, bilayer graphene, wrinkle, cluster

Although the investigation of graphene[1] (Gr) and its epitaxial growth[2] is a prime area of research in physics, chemistry, and materials science, little is known today about the interaction of carbon vapor with Gr at the microscopic level. This is surprising for several reasons.

First, deep insight into the structure and properties of defects in Gr was gained through transmission electron microscopy experiments, where the electron beam was used to create vacancy type defects by atom removal and to induce their transformations.[3–7] Experimental work on the reverse mechanism of defect creation, *i.e.*, the addition of C atoms (or small molecules) is scarce. Only Lehtinen *et al.*[8] and Robertson *et al.*[9] investigated a variety of self-interstitial atom configurations under the non-equilibrium conditions of energy transfer and sputtering by impinging energetic electrons.

Second, the condensation of carbon vapor on a substrate has been investigated as a route for Gr growth,[10–12] which is of specific interest for catalytically inactive substrates that do not allow the application of the usual chemical vapor phase deposition methods.[13,14] Surprisingly, condensation of carbon vapor *on* Gr as a substrate has not come into focus. Noteworthy exceptions are the early work of Tontegode and Rut'kov[15] as well as the more recent study of Nie *et al.*,[16] who investigated the high temperature exposure of Gr on Ir(111) to C vapor which yields additional Gr layers. The latter work presents evidence for the second Gr layer to nucleate from below.[16]

Third, as reactive C atoms (or small C molecules) can be expected to bind chemically to Gr at sufficiently low temperature, one could envision C deposition as an intermediate step to subsequent functionalization of Gr or even as a method to create new Gr hybrid materials.

In this Letter, using scanning tunneling microscopy (STM), density functional theory (DFT), as well as X-ray photoelectron spectroscopy (XPS), we investigate the processes and morphological effects arising from condensation of C vapor on single-crystalline graphene resting on Ir(111) as a function of the substrate temperature. At high temperatures, we find that C atoms not only permeate through the closed Gr sheet, giving rise to the growth of additional Gr layers underneath,[15,16] but also incorporate and densify the top Gr layer. When Gr is cooled to ambient, the extra incorporated C induces substantial wrinkling. At low temperatures, permeation and incorporation are blocked to good approximation. Instead C clusters *on top* of Gr form, being firmly attached to the Gr sheet. The clusters display a surprisingly regular array. We obtain insights into the structure and the binding of these clusters to graphene and study their transformation through heating.

Figure 1(a) displays a large-scale STM topograph, which serves as a reference for the evolution of a Gr layer on Ir(111) upon exposure to C vapor at high temperatures. The initial Gr layer is a single crystal sheet grown to complete closure of the metal surface. It is well aligned with the Ir(111) substrate, so that it forms a moiré of 2.5 nm periodicity with Ir(111) (see Methods Section). In the following it is referred to as the Gr cover. The Gr

cover was subsequently exposed to a carbon vapor flux at a sample temperature of 1170 K and for a duration that could have resulted in the formation of 0.8 monolayers (ML) of graphene. We note that the C vapor is composed not only of C monomers, but contains about twice as many C trimers (compare Methods Section). Figure 1(b) is a schematic representation of the resulting topography displayed in Figure 1(a), and it helps to distinguish between mono- (gray) and bilayer (blue) Gr areas. Characteristic features in Figure 1(a) are triangular bilayer islands, mostly with a bright bulge in their center, a wide stripe of bilayer Gr crossing the image and a network of bright lines. All bilayer Gr resulting from C deposition is formed *underneath* the covering Gr sheet, as has been demonstrated by Nie *et al.*[16] Under the conditions of preparation used here, Gr underneath grows with precisely the same orientation as the Gr cover. Thereby bilayer areas exhibit an enhanced moiré contrast facilitating their assignment. This can be seen in Figure 1(c) which displays a monolayer area (upper right) next to a bilayer area with enhanced moiré contrast. The arrow in Figure 1(c) highlights the location, where the underlayer island, formed as a result of C vapor exposure, has grown into an Ir step edge. The borderline displays a characteristic sawtooth pattern with moiré periodicity (compare ref. [17]). We note that depending on the conditions, also misoriented Gr grows underneath the cover, then giving rise to additional moirés.[18] The Supporting Information provides an example as Figure S1. Inspection of Figure 1(b) makes plain that the area of bilayer Gr is substantially smaller than an area fraction of 0.8 that one would expect from the deposited amount, consistent with the analysis of several STM topographs. In fact, a substantial fraction of C re-evaporates and is not incorporated into the sample. At deposition temperatures of 1370 K re-evaporation is found to be nearly complete.

Outstanding in Figure 1(a) are the many bright line segments (specifically in the large bilayer stripe) and even more the network of bright lines with three-armed branching points [black in the schematic in Figure 1(b)]. The network extends over the entire topograph and displays a preference to stay close to Ir substrate steps. These bright lines are wrinkles and folds in the Gr cover. As apparent from the profile displayed in Figure 1(d), the wrinkles

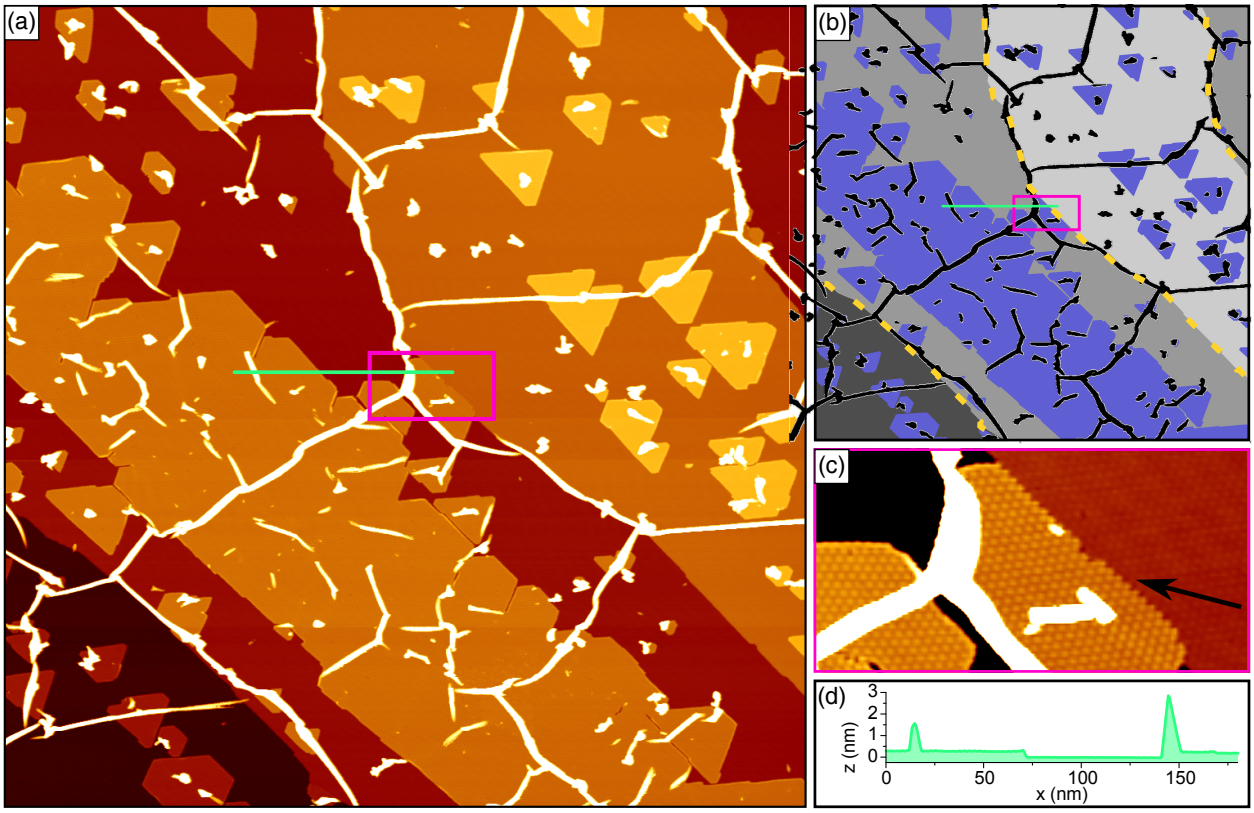

Figure 1: (a) STM topograph of Gr/Ir(111) after deposition of 0.8 ML C at 1170 K. (b) Schematic representation of (a): the position of Ir substrate steps of monatomic height are indicated by yellow dashed lines; the Ir terraces covered by monolayer Gr are shaded gray according to their height (light gray - highest terrace level, dark gray - lowest terrace level), bilayer Gr islands and areas are colored in blue and the position of wrinkles is indicated by black lines. (c) Magnified view of the area indicated in (a) and (b) by a pink box. The arrow indicates where an underlayer Gr island has grown into a preexisting Ir step. (d) Height profile along the green line indicated in (a) and (b). STM topograph sizes are (a) 680 nm × 680 nm and (c) 107 nm × 55 nm, respectively.

have a typical height of 2-3 nm. To highlight the significance of the wrinkles we evaluated their three-dimensional topography prior and after C deposition and found that compared to a Gr cover not exposed to C vapor, the additional wrinkles give rise to an extra, folded Gr area of (0.8±0.2) %.

Even without exposure to C vapor, occasional wrinkles are present in the Gr cover (compare Figure S2(a) of the Supporting Information). They originate from different thermal expansion coefficients of Gr and Ir. As the Gr cover is cooled from the high growth temperature, Ir shrinks, but Gr does not. Pinned to the substrate, Gr releases the resulting compressive strain partly by wrinkle formation.[19,20] The wrinkle density and induced extra Gr area are enhanced by more than a factor of three through the high temperature treatment of the Gr cover in C vapor (compare Figure S2(b) of the Supporting Information). Our observation therefore forces us to assume that after exposure to a C vapor additional C atoms are incorporated *into* the Gr cover on Ir(111), *i.e.*, after the C vapor treatment Gr is already compressed prior to the cool-down (compare also Figure S2(c) of the Supporting Information). This pre-straining is the origin of the enhanced wrinkling upon cooling.

To understand permeation *through* Gr and incorporation of C vapor *into* the Gr cover, we need to consider the energetics of the processes involved. If we set the energy of a C atom in a perfect Gr sheet on Ir(111) to $E_{\mathrm{Gr}} = 0\,\mathrm{eV}$, according to our DFT calculations the energy of a C atom in the vapor is $E_{\mathrm{v},1} = 8\,\mathrm{eV}$, the one of a C atom adsorbed on Gr $E_{\mathrm{on\ C},1} = 6.4\,\mathrm{eV}$ (the adsorption energy is thus $E_{\mathrm{ads},1} = 1.6\,\mathrm{eV}$), and the energy of the single C atom adsorbed on Ir(111) is $E_{\mathrm{on\ Ir},1} = 0.7\,\mathrm{eV}$[21] [compare Figure 2]. The corresponding numbers for a trimer are $E_{\mathrm{v},3} = 11\,\mathrm{eV}$ (assuming the trimer binding energy of 13 eV obtained by Raghavachari and Binkley[22]), $E_{\mathrm{on\ C},3} = 9.1\,\mathrm{eV}$, $E_{\mathrm{ads},3} = 1.9\,\mathrm{eV}$, and $E_{\mathrm{on\ Ir},3} = 3\,\mathrm{eV}$.[21]

These numbers imply an enormous decrease in energy upon permeation of vapor species through the Gr sheet to the Ir(111) surface, providing thereby the driving force for the growth of Gr islands underneath the Gr cover, as has already been pointed with qualitative arguments by Nie *et al.*[16] At the same time, these numbers imply also an even larger drop in

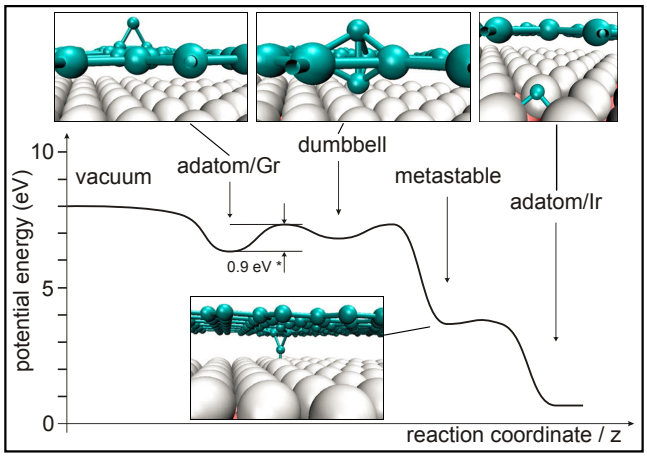

Figure 2: Energy for a carbon atom along a reaction coordinate from the vacuum to Ir(111) based on our DFT calculations. Zero energy corresponds to a C atom in a regular Gr lattice position. The insets display the C atom in the adatom to Gr, dumbbell, metastable, and adatom to Ir positions. The magnitude of the barrier indicated by * is taken from ref. 23.

energy upon incorporation of vapor phase species into regular lattice sites of the Gr cover.

Therefore, disregarding the details of the kinetic processes involved, we propose the following scenario: the C species condense from the supersaturated vapor on the hot Gr cover sheet, where they either re-evaporate (based on the numbers given above and with a pre-exponential factor ν_0 of 10^{12} the residence time τ can be estimated using the Arrhenius law $\frac{1}{\tau} = \nu_0 \cdot e^{-\frac{E_{ads,1}}{k_B \cdot T}}$, and is of the order of 10^{-5} s) or approach one of the two sinks for adsorbed C species: either regular sites in the Gr cover itself, or adsorption sites on Ir(111) in a 2D lattice gas of C species, from which eventually Gr islands nucleate, providing again regular lattice sites. It is important to note that the energy (chemical potential) of a C atom in a regular lattice site of the Gr cover rises due to the buildup of strain upon atom incorporation. Therefore, after some strain buildup, this sink ceases and the Gr cover will expel the same amount of C species to the Ir substrate that it incorporates from the adsorbed C, providing thereby the feed for underlayer Gr growth. This qualitative picture provides not only an explanation for the underlayer Gr growth, as has been observed before,[16] but also for the enhanced wrinkling in consequence of the Gr cover layer compression due to C species incorporation, which has been overlooked so far.

Due to the high sample temperature, the complexity of possible defect arrangements and transformations in Gr, and the presence of not only monomers but also trimers in the vapor, it is currently close to impossible to pinpoint with certainty *the* decisive atomic scale processes and their barriers for the above scenario. Nevertheless, it is instructive to consider possible candidates.

(i) Dislocation cores in Gr are associated with 5-7 defects, pentagon-heptagon pairs. Where Gr flakes join during the growth process, 5-7 defects are formed to accommodate slight misalignments.[13] Therefore these defects are always present to some extent in the Gr cover. When two migrating C atoms (migration barrier 0.5 eV[24]) meet at a 5-7 defect (the dislocation core), according to our *ab initio* calculations they are incorporated into the Gr network without any additional barrier and induce dislocation climb as illustrated in Figures 3(a) and (b). As the dislocation core is not changed upon atom incorporation, but only translated, the processes may be repeated again and again. Nevertheless, it is accompanied by gradual buildup of compressive strain in the Gr cover making incorporation energetically more and more costly. Dislocation climb by incorporation of vacancies, rather than adatoms, has been already been observed in transmission electron microscopy of Gr.[5,6]

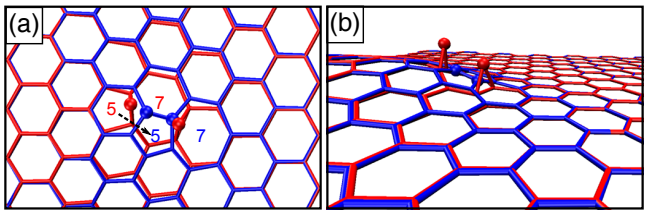

Figure 3: (a) Top and (b) side view of a dislocation core represented by a 5-7 defect before (red) and after (blue) spontaneous incorporation of the two C adatoms (red balls) and the resulting dislocation climb. The dashed arrow indicates the migration of the 5-membered C ring.

(ii) An adsorbed C adatom may reach the dumbbell configuration depicted in the inset of Figure 2 through overcoming a barrier of 0.9 eV.[23] From this metastable state, just 0.4 eV higher in energy than the adatom position (consistent with the result of Ma[23]) the atom dives without any noticeable barrier down to the Ir(111) substrate, where it contributes to

the buildup of a C adatom gas. Based on our numbers, the probability of a C atom to reach the dumbbell configuration within its lifespan is appreciable.

(iii) As DFT calculations[25] indicate, upon encounter of two migrating C adatoms on the perfect Gr lattice, an inverse Stone-Wales (ISW) defect can spontaneously form, without significant additional barrier and with a large energy gain of about 7 eV. The resulting ISW defect, consisting of two paired pentagons accompanied by two separate heptagons, deforms the Gr lattice substantially. For freestanding Gr, a bulge with a surrounding depression gives rise to a height amplitude of 2.7 Å.[25] Assuming a similar deformation for Gr on Ir(111), we can imagine an ISW defect to be the nucleus for incorporation of additional C species, resulting in larger deformations. From there C is expelled to the Ir substrate at the locations, where in consequence of deformation, Gr is pressed close to Ir. Indeed, nearly all triangular Gr islands grown underneath the Gr cover in Figure 1(a) carry in their center a bright bulge in plausible agreement with our speculation. We note that the bright bulges are in this view metastable, and consistent with this notion, do not form anymore for vapor deposition above 1300 K. We also remark that earlier transmission electron microscopy studies[9] suggested significant energy barriers for the formation of ISW defects, which could explain why bulges are not so frequent in the morphology.

Figure 4 (a) displays an STM topograph, which serves as a reference for the reaction of a Gr cover on Ir(111) upon exposure to C vapor at low temperatures, close to ambient. At 400 K the sample was exposed to 0.1 ML carbon vapor, an amount corresponding to an average of 21 C atoms per moiré unit cell. Based on the computed adsorption energies of $E_{\mathrm{ads},1} = 1.6\,\mathrm{eV}$ and $E_{\mathrm{ads},3} = 1.9\,\mathrm{eV}$, re-evaporation must be considered to be absent. Apparently, the deposited C largely remained *on* the Gr cover and was subject to a self-organization process. The resulting clusters are arranged with the moiré periodicity and form an imperfect C cluster lattice. In Figure 4 (a) less than 2 % of the moiré unit cells are empty, about 5 % of the clusters are misplaced on interstitial positions, and few clusters extend over two unit cells. The apparent size of the clusters varies considerably, indicated

by the height variation from 1 Å to 10 Å with an average of 3 Å. This implies a substantial variation of the number of C atoms forming the clusters. The order of the cluster lattice is inferior to the one of lattices formed by Ir, Pt, W, or Rh on Gr/Ir(111), but superior to one of other metals like Fe, Au, Co.[26] At 400 K, pronounced cluster lattices are observed for C exposures up to 0.3 ML. For larger amounts the clusters grow too large, and eventually touch or coalesce, whereby loss of order is induced.

The clusters result from diffusion of the deposited C species to locations within the moiré unit cell, where they bind more strongly to the Gr cover and aggregate. For the given deposition rate (see Methods Section), optimum order in the C cluster lattice is achieved in the temperature range from 300 K to 400 K. At 130 K order is lost, due to a lack of C species diffusion, while at 550 K the amount of empty moiré cells is increased, due to enhanced C species diffusion. Based on the analysis in Figure 4 (b), the clusters bind to the hcp-areas in the moiré (as do metal clusters[26,27]). In an hcp-area, an Ir(111) hcp threefold hollow site is in the center of the Gr C ring; thus three of the C atoms in a ring sit atop of Ir surface atoms. Though after deposition of very small amounts, *e.g.*, 0.03 ML, clusters can be removed by the STM tip, after deposition of 0.1 ML or more, clusters are strongly bound and cannot be manipulated by the STM tip. Their stability allows one to image them with relatively low tunneling resistance, such that molecular orbital resolution is achieved, as displayed in Figure 4 (c). The molecular structure of the clusters as imaged by STM resembles strikingly the one of C_{60} molecules imaged with a C_{60} functionalized tip by Lakin *et al.*[28] This may be due to sp^2 C fragments adsorbed to the tip and would imply a predominantly fullerene-like sp^2 type cluster structure. The cluster motifs of the topograph bear also similarity to STM images of the sp^2 shell of nanodiamonds as observed by Pawlak *et al.*[29]

To gain insight into the cluster binding mechanism, we collected XP spectra of Gr/Ir(111) before and after deposition of 0.3 ML C. This amount ensures a strong XPS signal and still results in a well-ordered C cluster array. The bottom panel of Figure 4 (d) displays the sharp C 1s peak prior to C deposition at a binding energy (BE) of 248.1 eV and an experimental

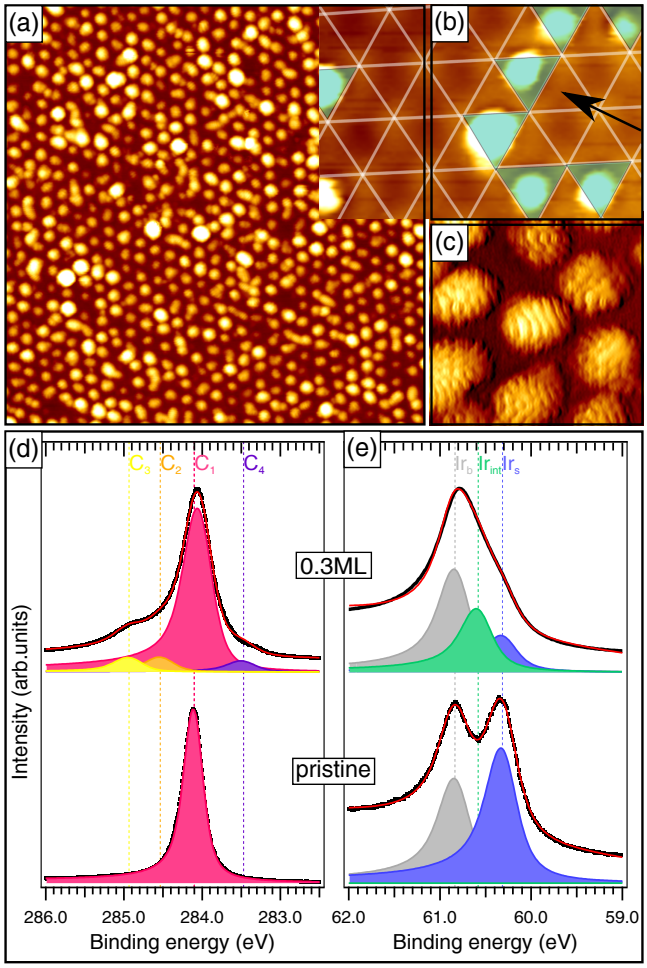

Figure 4: (a) STM topograph of the C cluster lattice on Gr/Ir(111) after exposure to 0.1 ML C vapor at 400 K. Image size is 60 nm × 60 nm. (b) STM topograph after exposure of Gr/Ir(111) to 0.03 ML C vapor at 400 K. The only partly occupied moiré allows one to draw a hexagonal network connecting the bright top-areas (in these areas an Ir atop site is located in the center of a C ring, compare ref. 27). The clusters are positioned in down-pointing triangles of the network. Together with the known crystal orientation (the $[\bar{1}\bar{1}2]$-direction is indicated), this implies cluster adsorption in the hcp-areas of the moiré. Image size is 8.5 nm × 8.5 nm. (c) STM topograph after 0.1 ML C deposition on Gr/Ir(111) at 400 K with molecular orbital cluster resolution obtained by imaging with relatively low tunneling resistance; $U_s = 1.5$ V, $I_t = 0.6$ nA. Image size is 7.5 nm × 7.5 nm. (d) XP spectra of the C 1s peak of pristine Gr/Ir(111) (lower spectrum) and after additional 0.3 ML C deposition (upper panel) fitted with four components (see text). (e) Ir $4f_{7/2}$ spectra of pristine Gr/Ir(111) (lower panel) and after additional 0.3 ML C deposition (upper panel). The spectra display the bulk peak Ir_b, the surface peak Ir_s, and an additional component Ir_{int}, due to chemical interaction after C deposition (see text).

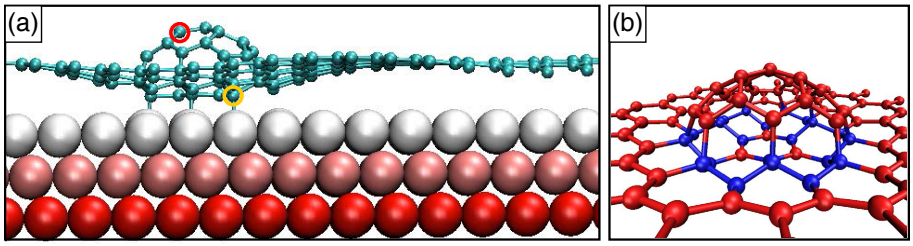

Figure 5: (a) Side view for the DFT-optimized geometry of a 19 C atom cluster in the hcp-area of Gr/Ir(111). Encircled are a C atom of the cluster (red) and a C atom of the rehybridized area underneath the cluster (yellow). See text. (b) Perspective view of the same system as in (a), but with the C atoms colored according to their coordination: red for 3 neighbors (counting bonds to Ir atoms) and blue for 4 neighbors. Ir substrate atoms are not shown for clarity.

Gaussian full width at half maximum (GFWHM) of 0.21 eV. It is well reproduced through a single fit component C_1 (magenta), in agreement with previous work.[30] After C deposition, the predominant intensity of the C 1s peak is still reproduced by a broadened (GFWHM of 0.37 eV) and slightly shifted (-0.1 eV) C_1 component [upper panel in Figure 4 (d)]. We attribute these changes to variations in the chemical environment and doping of the sp^2 hybridized Gr atoms.

Moreover, the experimental spectrum displays a high-energy shoulder. Diamond-like sp^3 carbon is characterized by a C 1s component in the range of 284.9 eV[31] to 285.2 eV[32] roughly matching the position of the high-energy shoulder. At the same time, a similar shoulder ("rehybridization shoulder") has previously been observed after metal cluster adsorption on Gr/Ir(111) and was attributed to Gr atoms rehybridized underneath and in the vicinity of the metal clusters to sp^3 carbon.[30,33] In principle both effects could contribute to the formation of this shoulder, and their origin will be reanalyzed below with additional information. To adequately fit the high-energy shoulder, two additional components C_2 (orange) and C_3 (yellow) must be introduced, similar to the rehybridization shoulder.[30]

Finally, also towards the low-energy side the experimental spectrum develops a tiny shoulder accounted for in the fit through a component C_4 (purple) at a BE of 283.45 eV. This shoulder is absent in the C 1s spectrum after metal cluster growth. We interpret

this component to be due to carbidic carbon, *i.e.*, carbon chemisorbed to Ir.[34] After ion irradiation of Gr/Ir(111), creating detached C atoms, a similar intensity increase at the low binding energy side is observed, consistent with our assignment. The component C_4 thus seems to indicate that a small amount of carbon – presumably monomers – permeated the Gr sheet even at 400 K deposition temperature, *e.g.*, by mechanism (ii) mentioned above.

The Ir $4f_{7/2}$ spectrum of pristine Gr/Ir(111) displayed as the bottom panel in Figure 4 (e) features two components. The component at a BE of 60.8 eV is assigned to Ir bulk atoms (Ir_b) whereas the component at a BE of 60.3 eV originates from the surface atoms (Ir_s) consistent with literature.[35] Upon C deposition the surface component Ir_s is strongly reduced [upper panel of Figure 4 (e)] and a third component Ir_{int} at a BE of 60.5 eV has to be introduced for a reasonable fit. The Ir_{int} component must be attributed to Ir surface atoms now interacting chemically with the C. The large spectral weight of the Ir_{int} component suggests that it is made up of Ir atoms binding to rehybridized C atoms and Ir atoms bound to permeated C monomers.

DFT calculations, though unable to explore the configuration space to any reasonable extent, are nevertheless instructive to understand the link between cluster binding and cluster structure. First we joined 16 and 58 atom clusters of sp^3 diamond to the hcp-areas. After relaxation the energies per C atom were 2.0 eV and 1.33 eV, respectively. For 10 and 19 atom clusters consisting of sp^2 hybridized flakes that were joined as hemispherical caps to Gr/Ir(111) in the hcp-areas, the energies per C atom were 1.6 eV and 1.0 eV, respectively, much lower as for the diamond clusters of comparable size. Figure 5 (a) displays a side view of the 19 atom cluster forming a fullerene type hemispherical cap on the Gr cover. It is apparent that the Gr sheet bends down towards the substrate at the cluster location. This is enabled in the hcp-areas with Gr C atoms sitting atop of Ir atoms. There $C(2p_z)$ orbitals hybridize with the $Ir(5d_{3z^2-r^2})$ orbitals and form chemical bonds.[36] In the perspective view of Figure 5 (b) the threefold coordinated sp^2 type C atoms are colored red, while the fourfold coordinated sp^3 hybridized C atoms (including bonds to the Ir substrate not shown) are

colored blue. Results for the other cluster sizes are provided as Figure S3 in the Supporting Information. Based on its low energy, we are convinced that the 19 atom cluster represented by Figure 5 (a) and (b) is a typical case.

A consistent interpretation of the XP spectra in the light of the DFT calculations is obtained by assuming that (i) the majority of deposited C atoms contributes to the C_1 peak of sp^2 hybridized carbon (fullerene-type carbon), (ii) some carbon, presumably deposited monomers, still permeate to the Ir substrate giving rise to the C_4 component and contributing through their binding to Ir to Ir_{int}, (iii) rehybridization of C atoms in the Gr cover gives rise to the majority of intensity in the C_2 and C_3 components. Since components C_2 and C_3 are still small after deposition of 1 ML C atoms, we rule out that a significant part of the deposited C atoms is sp^3 hybridized. Together with the molecular orbital appearance of the clusters, these arguments provide evidence for a fullerene-type hemispherical cap structure of the clusters.

It is not surprising that the deposited C is predominantly present in sp^2 hybridized form. Surfaces of sp^3 bonded diamond reconstruct involving π-bonding,[37] driven by the removal of energetically costly dangling bonds. For the same reason, also amorphous carbon films display at their surface predominantly sp^2 bonding.[38] For the present case, we imagine that in the hcp areas, where hybridization is facile, C trimers and C atoms attach. Thereby growth normal to the Gr cover is induced. In order to minimize the system energy, there will be a strong tendency of subsequently arriving C species to reduce the energy associated with the resulting dangling bonds, *i.e.*, to connect different C atoms and atom groups and thereby to remove dangling bonds. This leads directly to sp^2 bonding motifs resulting in configurations similar to the hemispherical fullerene cap.

Contrary to the interpretation given here, one might propose that the C clusters form *underneath* the Gr sheet. Indeed, in view of the tiny component C_4 a small amount of carbon atoms may have penetrated the Gr cover and be adsorbed to Ir(111), presumably as monomers. However, we rule out that the clusters seen in the STM topographs are grown

underneath the Gr cover for the following reasons: (i) As mentioned above, small clusters can be picked up by the STM tip, providing direct evidence for the formation on top of the Gr sheet. (ii) Considering the average apparent cluster height of 3 Å, formation underneath would imply a large deformation energy in the Gr cover. (iii) Clusters form in the hcp-areas, where the Gr cover has been shown to be most sticky to arriving particles and where it binds strongest to the substrate. Cluster formation underneath would be expected in the top areas, where the Gr does not bind to the substrate[36] and provides space for intercalation. (iv) The vast majority of carbon arrives as trimers on the Gr sheet, for which penetration barriers much larger than the 0.9 eV calculated for monomers must be assumed. (v) We will see in the next section that some clusters survive up to annealing temperatures of 1350 K, a temperature at which any C cluster in contact with Ir would have readily transformed to Gr.[39]

According to our DFT calculations, the C clusters adsorbed on Gr/Ir(111) have energies on the order of 1 eV and are thus metastable configurations with respect to Gr. Annealing is therefore likely to transform the clusters to lower energy configurations, *e.g.*, to Gr.

Figure 6 presents STM results of an annealing sequence, starting (a) after exposure od Gr/Ir(111) to 0.3 ML of C at 400 K, and after isochronal annealing for 60 s to (b) 600 K, (c) 800 K, (d) 1000 K, (e) 1200 K, and (f) 1350 K. The filling factor (number of clusters per moiré unit cell) is initially close to 100 %, remains almost constant up to 800 K (90 %), and then decreases gradually with increasing temperature. Four qualitative features are remarkable in the annealing sequence: (1) With increasing annealing temperature there is only cluster disappearance, but no ripening, *i.e.*, there is no growth of some clusters at the expense of others. This is contrary to what is found for metal clusters on Gr/Ir(111) which display a clear ripening through cluster diffusion and coalescence (Smoluchowski ripening).[26,33] (2) Starting already at 800 K and well visible after annealing to 1000 K, flat platelets of uniform height are visible, which grow in area and decrease in number with increasing annealing temperature. These flat platelets result from underlayer Gr. Their height of 3 Å, the growth

of the platelets into preexisting substrate steps, and the characteristic sawtooth pattern with moiré periodicity of the grown in edge in Figure 6(f) (see arrow) leave no doubt that the majority of clusters transformed into bilayer Gr during heating. (3) It is surprising that some clusters have already disappeared at the lowest annealing temperature, while many others survive up to 1200 K. This broad temperature range of disappearance indicates that the cluster stability strongly depends on the precise cluster configuration. (4) Some clusters remain on bilayer areas. It is no coincidence that in Figure 6(f) the only clusters left are found on the bilayer Gr island.

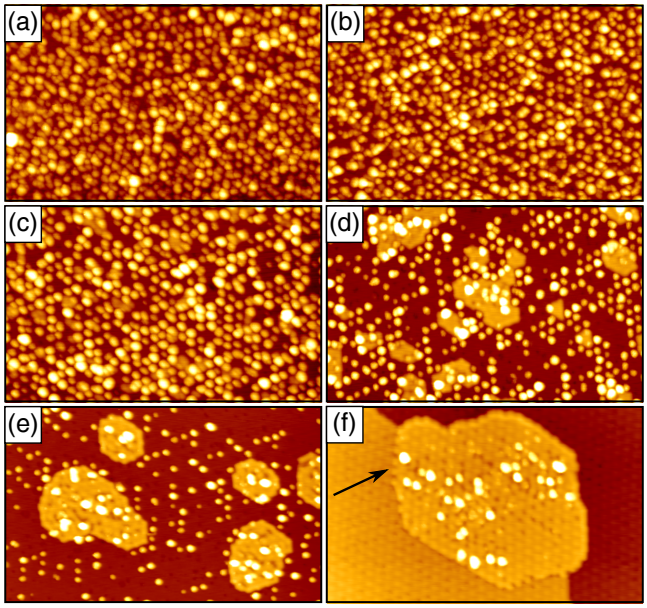

Figure 6: (a) STM topograph of 0.3 ML C deposited on Gr/Ir(111) at 400 K and subsequently annealed to (b) 600 K, (c) 800 K, (d) 1000 K, (e) 1200 K, and (f) 1350 K. Image sizes are 80 nm $\times$ 50 nm. The arrow in (f) indicates the characteristic sawtooth pattern with moiré periodicity of the grown in edge.

Our observations may be rationalized by viewing the clusters as not being adsorbed to the Gr cover, but by assuming that the system consists of C clusters adsorbed to the Ir(111) substrate, which are joined by Gr: each adsorbed C aggregate forms with the underlying piece of diamond-like carbon (emerging from local rehybridization of the Gr cover) an inseparable unit. Clusters cannot merge as they are fixed by Gr spacers, *i.e.*, Smoluchowski ripening is prohibited. Detachment and reattachment of C atoms does not take place for C atoms in

the upper part of the cluster [*e.g.*, the C atom encircled red in Figure 5(a)], where it could lead to Ostwald ripening of the clusters, because a C atom detachment would involve an increase of the system energy of the order of 5 eV [compare Figure 2] before the atom could reincorporate. Only for those C atoms already in direct contact with Ir(111) [*e.g.*, the C atom encircled yellow in Figure 5(a)], detachment and hence adsorption on the substrate can take place, as due to the close proximity of the substrate being a low energy sink, a low energy transition state exists. Out of these C atoms the underlayer Gr nucleates and grows until the excess C in the clusters is consumed, such that the cover is eventually restored as a Gr sheet. As the clusters are not all alike, the barriers for C atom detachment to the Ir surface will vary considerably, explaining the broad temperature range of gradual cluster disappearance [observation (3)]. In case underlayer Gr has grown under the Gr cover still containing clusters, the clusters' contact to Ir is lost. Thereby the driving force for C atom detachment is lost, and the cluster decay is prevented [observation (4)]. Since in this case the upper Gr layer is detached from the Ir(111) substrate and can be viewed as quasi-freestanding it must be concluded, that the C cluster stability does not depend on the Ir substrate, *i.e.*, once formed on the Gr cover the clusters will be stable even without the Ir substrate.

In conclusion, our experiments and simulations uncover two new phenomena caused by the interaction of C vapor with Gr on a metal. First, exposure to C vapor at high temperatures gives rise to drastically enhanced wrinkling in the Gr cover after cool down. The origin of the enhanced wrinkling was traced back to the fact that C vapor not only permeates through the Gr cover, but also remains within and densifies the Gr. Second, exposure to carbon vapor at ambient temperatures gives rise to the formation of carbon clusters, which form a regular lattice with the periodicity of the moiré of the underlayer graphene with Ir(111). The C clusters are segments of fullerene-type structures bound to the Gr cover. At their baseline substantial rehybridization of the Gr cover to sp^3, diamond-like carbon takes place. The enormous thermal stability of the C clusters is due to the absence of ripening. They eventually decay by C exchange with the Gr cover which itself feeds the interface with

C atoms that aggregate to Gr underlayer islands.

The exposure of Gr to a C vapor is a strong lever to modify the properties of Gr and to create new Gr hybrid materials. To fully exploit the potential of the interaction of elemental carbon with Gr, in the future it will be important to employ pure vapors of C monomers, C dimers, C trimers, *etc.* This would enable to pin down specific reaction paths, and thus to unambiguously link experiment with modeling resulting in a predictive understanding.

On the negative side, our research indicates that Gr bilayer growth from the C vapor is an unsuitable method for achieving high quality material. For the purpose of bi-layer growth segregation from bulk carbon[18,40–42] is more suited as it avoids permeation, thus the associated partial C incorporation into the cover layer, and in consequence the enhanced wrinkling.

On the positive side, after removal of the graphene/ C-cluster hybrid from its substrate, *e.g.*, through the H_2-bubbling method,[43] we have a new, regularly nanostructured, ultra-thin carbon material at hand. Due to the nanostructured surface, it appears plausible that this material stably binds deposited metal, *e.g.*, Pt, in a finely dispersed way as small clusters. As the material is predominantly sp^2 hybridized, it should also display good corrosion resistance as an electrode, properties that let our new material appear attractive as a catalyst electrode in fuel cells.[44–46] Another potential application of our work could be the encapsulation of regular metal cluster arrays on graphene by subsequent carbon vapor exposure and annealing.

Methods

STM and XPS experiments were conducted in ultra high vacuum systems in Cologne and at the I311 beamline[47] of Max IV Laboratory in Lund, respectively. Prior to each experiment Ir(111) was cleaned by cycles of room temperature noble gas sputtering and flash annealing. Initially, the sample was also treated by O_2 exposure and sputtering at elevated temperature ($\approx 1000\,\mathrm{K}$). A fully closed, well-oriented, monolayer Gr sheet was prepared by room tem-

perature ethylene adsorption until saturation, thermal decomposition at 1470 K (Cologne) or 1300 K (Lund), and subsequent high temperature exposure (1270 K in Cologne, 1170 K in Lund) to ethylene.[48]

Carbon vapor was created by sublimation from a C rod, e-beam heated to ≈ 2250 K. The C deposition rate was about 1×10^{17} atoms $m^{-2}s^{-1}$ and determined by room temperature deposition, subsequent annealing for Gr formation, and surface area analysis by STM. The integrated C exposure is specified in monolayers (ML), where 1 ML corresponds to 3.8×10^{19} atoms m^{-2}, which is the areal atomic density of a Gr layer. Based on the data of Zavitsanos and Carlson[49] and at the experimental evaporation temperature, the number of C trimers in the vapor is about twice as high as the one of C monomers, while the number of C dimers is measurably small and all other clusters sizes are marginal.

STM imaging was conducted at room temperature with a typical sample bias U_s ranging from -2 V to +5 V and a tunneling current of $I_t \approx 0.5$ nA.

XP spectra were recorded at room temperature in normal emission. C 1s core levels were measured using a photon energy of 390 eV with a total energy resolution better than 60 meV. Ir 4f core levels were measured with a photon energy of 120 eV and a total energy resolution better than 45 eV.

The first-principles DFT calculations were performed using the plane-wave-basis-set Vienna *ab initio* simulation package.[50,51] The projector augmented wave approach[52] was used to describe the core electrons and a non-local van der Waals functional[53] to describe exchange and correlation. A plane wave kinetic energy cutoff of 400 eV was found to converge energy differences between different configurations within 0.1 eV, which was sufficient for calculating energy differences between different configurations. The same accuracy was achieved with regard to the number of k-points ($3 \times 3 \times 1$) in the two-dimensional Brillouin zone. All structures were relaxed until atomic forces were below 0.002 eV/Å. The calculations were carried out for a 200-atom 10×10 Gr supercell on top of a 9×9 three-atomic-layer-thick Ir(111) slab containing 243 atoms, as in our previous work,[54,55] or for the same Ir slab without Gr.

20 Å of vacuum was added in the transverse direction to separate the periodic images of the slab.

Supporting Information Available

The Supporting Information contains as Figure S1 an STM topograph of bilayer Gr on Ir(111), where the undercover Gr island has a slight misorientation with respect to the cover, as Figure S2 a comparison between Gr exposed and not exposed to C vapor at high temperature together with a sketch of the changes due to cool down, and finally as Figure S3 graphical representations for DFT calculations of carbon clusters on Gr/Ir(111) with 10, 16, and 58 atoms. This material is available free of charge via the Internet at `http://pubs.acs.org/`.

Acknowledgement

Financial support of the DFG through project MI581/22-1 *Low energy ion irradiation of 2D-materials*, of the Bonn-Cologne Graduate School for Physics and Astronomy (C. H.), of the European Commission under a Marie-Skłodowska-Curie fellowship (A. J. M.-G.), of the Swedish Research Council through project 2012-3850 (J. K.), and of the Alexander von Humboldt-Stiftung (C. T.) is gratefully acknowledged. A.V.K. acknowledges Academy of Finland funding through project 286279.

References

(1) Novoselov, K. S.; Geim, A. K.; Morozov, S. V.; Jiang, D.; Zhang, Y.; Dubonos, S. V.; Grigorieva, I. V.; Firsov, A. A. *Science* **2004**, *306*, 666–669.

(2) Tetlow, H.; Boer, J. P. D.; Ford, I. J.; Vvedensky, D. D.; Coraux, J.; Kantorovich, L. *Phys. Rep.* **2014**, *542*, 195–295.

(3) Hashimoto, A.; Suenaga, K.; Gloter, A.; Urita, K. *Lett. to Nat.* **2004**, *430*, 17–20.

(4) Kotakoski, J.; Krasheninnikov, A. V.; Kaiser, U.; Meyer, J. C. *Phys. Rev. Lett.* **2011**, *106*, 105505.

(5) Warner, J. H.; Margine, E. R.; Mukai, M.; Robertson, A. W.; Giustino, F.; Kirkland, A. I. *Science* **2012**, *337*, 209–212.

(6) Lehtinen, O.; Kurasch, S.; Krasheninnikov, A. V.; Kaiser, U. *Nat. Commun.* **2013**, *4*, 2098.

(7) Robertson, A. W.; Lee, G.-D.; He, K.; Yoon, E.; Kirkland, A. I.; Warner, J. H. *Nano Lett.* **2014**, *14*, 1634–1642.

(8) Lehtinen, O.; Vats, N.; Algara-Siller, G.; Knyrim, P.; Kaiser, U. *Nano Lett.* **2014**, *15*, 235–241.

(9) Robertson, A. W.; He, K.; Kirkland, A. I.; Warner, J. H. *Nano Lett.* **2014**, *14*, 908–914.

(10) Park, B. J.; Mitchel, W. C.; Grazulis, L.; Smith, H. E.; Eyink, K. G.; Boeckl, J. J.; Tomich, D. H.; Pacley, S. D.; Hoelscher, J. E. *Adv. Mater.* **2010**, *22*, 4140–4145.

(11) Wurstbauer, U.; Schiros, T.; Jaye, C.; Plaut, A. S.; He, R.; Fischer, D.; Pfeiffer, L. N.; Rigosi, A.; Gutie, C.; Pasupathy, A. N.; Pinczuk, A.; Garcia, J. M. *Carbon* **2012**, *50*, 4822–4829.

(12) Oliveira, M. H.; Schumann, T.; Gargallo-Caballero, R.; Fromm, F.; Seyller, T.; Ramsteiner, M.; Trampert, A.; Geelhaar, L.; Marcelo, J.; Lopes, J.; Riechert, H. *Carbon* **2013**, *56*, 339–350.

(13) Coraux, J.; N'Diaye, A. T.; Busse, C.; Michely, T. *Nano Lett.* **2008**, *8*, 565–570.

(14) Li, X.; Cai, W.; An, J.; Kim, S.; Nah, J.; Yang, D.; Piner, R.; Velamakanni, A.; Jung, I.; Tutuc, E.; Banerjee, S. K.; Colombo, L.; Ruoff, R. S. *Science* **2009**, *324*, 1312.

(15) Tontegode, A. Y.; Rut'kov, E. V. *Phys. - Uspekhi* **1993**, *36*, 1053–1067.

(16) Nie, S.; Walter, A. L.; Bartelt, N. C.; Starodub, E.; Bostwick, A.; Rotenberg, E.; McCarty, K. F. *ACS Nano* **2011**, *5*, 2298–2306.

(17) N'Diaye, A. T.; Coraux, J.; Plasa, T. N.; Busse, C.; Michely, T. *New J. Phys.* **2008**, *10*, 043033.

(18) Que, Y.; Xiao, W.; Fei, X.; Chen, H.; Huang, L.; Du, S. X.; Gao, H.-J. *Appl. Phys. Lett.* **2014**, *104*, 093110.

(19) N'Diaye, A. T.; Gastel, R. V.; Martínez-Galera, A. J.; Coraux, J.; Hattab, H.; Wall, D.; Meyer zu Heringdorf, F.-J.; Horn-von Hoegen, M.; Gómez-Rodríguez, J. M.; Poelsema, B.; Busse, C.; Michely, T. *New J. Phys.* **2009**, *11*, 113056.

(20) Hattab, H.; N'Diaye, A. T.; Wall, D.; Klein, C.; Jnawali, G.; Coraux, J.; Busse, C.; van Gastel, R.; Poelsema, B.; Michely, T.; zu Heringdorf, F.-J. M.; Horn-von Hoegen, M. *Nano Lett.* **2012**, *12*, 678–682.

(21) Herbig, C.; Åhlgren, E. H.; Jolie, W.; Busse, C.; Kotakoski, J.; Krasheninnikov, A. V.; Michely, T. *ACS Nano* **2014**, *8*, 12208–12218.

(22) Raghavachari, K.; Binkley, J. S. *J. Chem. Phys.* **1987**, *87*, 1987.

(23) Ma, Y. *Phys. Rev. B* **2007**, *76*, 075419.

(24) Lehtinen, O.; Foster, A. S.; Ayuela, A.; Krasheninnikov, A. V.; Nordlund, K.; Nieminen, R. M. *Phys. Rev. Lett.* **2003**, *91*, 017202.

(25) Lusk, M. T.; Wu, D. T.; Carr, L. D. *Phys. Rev. B* **2010**, *81*, 155444.

(26) N'Diaye, A. T.; Gerber, T.; Busse, C.; Mysliveček, J.; Coraux, J.; Michely, T. *New J. Phys.* **2009**, *11*, 103045.

(27) N'Diaye, A. T.; Bleikamp, S.; Feibelman, P.; Michely, T. *Phys. Rev. Lett.* **2006**, *97*, 215501.

(28) Lakin, A. J.; Chiutu, C.; Sweetman, A. M.; Moriarty, P.; Dunn, J. L. *Phys. Rev. B* **2013**, *88*, 035447.

(29) Pawlak, R.; Glatzel, T.; Pichot, V.; Schwidlin, L.; Kawai, S.; Fremy, S.; Spitzer, D.; Meyer, E. *Nano Lett.* **2013**, *13*, 5803–5807.

(30) Knudsen, J.; Feibelman, P.; Gerber, T.; Grånäs, E.; Schulte, K.; Stratmann, P.; Andersen, J. N.; Michely, T. *Phys. Rev. B* **2012**, *85*, 035407.

(31) Chavanne, A.; Arnault, J.-C.; Barjon, J.; Arabski, J. *Surf. Sci.* **2011**, *605*, 564–569.

(32) Mérel, P.; Tabbal, M.; Chaker, M.; Moisa, S.; Margot, J. *Appl. Surf. Sci.* **1998**, *136*, 105–110.

(33) Gerber, T.; Knudsen, J.; Feibelman, P. J.; Granas, E.; Stratmann, P.; Schulte, K.; Andersen, J. N.; Michely, T. *ACS Nano* **2013**, *7*, 2020–2031.

(34) Rey, S.; Le Normand, F. *Thin Solid Films* **2011**, *519*, 4426–4428.

(35) Bianchi, M.; Cassese, D.; Cavallin, a.; Comin, R.; Orlando, F.; Postregna, L.; Golfetto, E.; Lizzit, S.; Baraldi, a. *New J. Phys.* **2009**, *11*, 063002.

(36) Busse, C.; Lazić, P.; Djemour, R.; Coraux, J.; Gerber, T.; Atodiresei, N.; Caciuc, V.; Brako, R.; N'Diaye, A. T.; Blügel, S.; Zegenhagen, J.; Michely, T. *Phys. Rev. Lett.* **2011**, *107*, 036101.

(37) Ristein, J. *Surf. Sci.* **2006**, *600*, 3677–3689.

(38) Jackson, S. *Appl. Surf. Sci.* **1995**, *90*, 195–203.

(39) Coraux, J.; N'Diaye, A. T.; Engler, M.; Busse, C.; Wall, D.; Buckanie, N. M.; Meyer zu Heringdorf, F.-J.; van Gastel, R.; Poelsema, B.; Michely, T. *New J. Phys.* **2009**, *11*, 023006.

(40) Sutter, P.; Sadowski, J. T.; Sutter, E. *Phys. Rev. B* **2009**, *80*, 245411.

(41) Nie, S.; Wu, W.; Xing, S.; Yu, Q.; Bao, J.; Pei, S.-S.; McCarty, K. F. *New J. Phys.* **2012**, *14*, 093028.

(42) Li, J.; Zhou, G.; Chen, Y.; Gu, B.-L.; Duan, W. *J. Am. Chem. Soc.* **2009**, *131*, 1796–1801.

(43) Gao, L.; Ren, W.; Xu, H.; Jin, L.; Wang, Z.; Ma, T.; Ma, L.-P.; Zhang, Z.; Fu, Q.; Peng, L.-M.; Bao, X.; Cheng, H.-M. *Nat. Commun.* **2012**, *3*, 699.

(44) Debe, M. K. *Nature* **2012**, *486*, 43–51.

(45) Wang, X. X.; Tan, Z. H.; Zeng, M.; Wang, J. N. *Sci. Rep.* **2014**, *4*, 4437.

(46) Lim, K. H.; Oh, H.-S.; Kim, H. *Electrochem. commun.* **2009**, *11*, 1131–1134.

(47) Nyholm, R.; Andersen, J. N.; Johansson, U.; Jensen, B. N.; Lindau, I. *Nucl. Instruments Methods Phys. Res. A* **2001**, *467-468*, 520–524.

(48) van Gastel, R.; N'Diaye, A. T.; Wall, D.; Coraux, J.; Busse, C.; Buckanie, N. M.; Meyer zu Heringdorf, F.-J.; Horn von Hoegen, M.; Michely, T.; Poelsema, B. *Appl. Phys. Lett.* **2009**, *95*, 121901.

(49) Zavitsanos, P. D.; Carlson, G. A. *J. Chem. Phys.* **1973**, *59*, 2966.

(50) Kresse, G.; Furthmüller, J. *Comput. Mater. Sci.* **1996**, *6*, 15–50.

(51) Kresse, G.; Furthmüller, J. *Phys. Rev. B* **1996**, *54*, 11169–11186.

(52) Blöchl, P. E. *Phys. Rev. B* **1994**, *50*, 17953–17979.

(53) Björkman, T. *Phys. Rev. B* **2012**, *86*, 165109.

(54) Standop, S.; Lehtinen, O.; Herbig, C.; Lewes-Malandrakis, G.; Craes, F.; Kotakoski, J.; Michely, T.; Krasheninnikov, A. V.; Busse, C. *Nano Lett.* **2013**, *13*, 1948–1955.

(55) Blanc, N.; Jean, F.; Krasheninnikov, A. V.; Renaud, G.; Coraux, J. *Phys. Rev. Lett.* **2013**, *111*, 085501.

Graphical TOC Entry